the catalytic action. It is still not clear by what mechanism the H is activated by the tip and transferred to the carbonaceous fragments. It is known that hydrogen readily dissociates over platinum even below 300 K, as shown by H_2-D_2 exchange studies (*10*). Because the residence time of the tip over the area occupied by one cluster is on the order of milliseconds at our scanning speeds, the turnover frequency of the H transfer reaction from the tip is about 2×10^3 s^{-1} per Pt site (assuming the atoms are being transferred from a single Pt atom on the STM tip). This is about an order of magnitude higher than that expected from comparable studies of the hydrogenation of ethylene and propylene under similar conditions (*11*) and several orders of magnitude higher than hydrogenolysis of C_xH_y species (*12*). However, these differences are not surprising because it is not necessary for these molecules to be completely hydrogenated and removed from the surface in order for them to be unobservable by the STM.

Isotope exchange reactions of hydrocarbons with deuterium gas on Pt(111) have shown that the exchange kinetics at low conversions displayed zero activation energy, a first-order dependence on D_2 pressure, and a strong negative-order dependence on the surface coverage by strongly bound carbonaceous species (*13*, *14*). This negative-order dependence arises from the inhibition of dissociative chemisorption of deuterium molecules by the carbonaceous deposits. It was found that the rate of dissociative deuterium chemisorption on the platinum surfaces that are partially covered by strongly chemisorbed carbonaceous species controlled the overall exchange kinetics. From these observations, it could be argued that in our case, the STM tip acted as a source of activated hydrogen, eliminating the need for a site for dissociative hydrogen chemisorption on the surface and, as a result, significantly increased the rate of conversion of the hydrocarbon clusters.

We believe that these results demonstrating the catalytic action of the STM tip open the way for experiments that will allow the study of the local catalytic activity of surface sites and defects that can at present only be studied in an average way with the more conventional tools and methods.

REFERENCES AND NOTES

1. B. J. McIntyre, M. Salmeron, G. A. Somorjai, *Rev. Sci. Instrum.* **64**, 687 (1993).
2. ———, *J. Vac. Sci. Technol. A* **11**, 1964 (1993).
3. Ph. Avouris, *Atomic and Nanometer-Scale Modification of Materials: Fundamentals and Applications*, Ph. Avouris, Ed. (NATO Advanced Studies Institute Series E, no. 239, Kluwer Academic, Boston, MA, 1993).
4. D. M. Zeglinski *et al.*, *Rev. Sci. Instrum.* **61**, 3769 (1990).
5. For a few references describing structural observations of propylidyne, see M. Salmeron and G. A. Somorjai, *J. Phys. Chem.* **86**, 341 (1982); R. J. Koestner, M. A. Van Hove, G. A. Somorjai, *ibid.* **87**, 203 (1983); R. J. Koestner, J. C. Frost, P. C. Stair, M. A. Van Hove, G. A. Somorjai, *Surf. Sci.* **116**, 85 (1982); K. M. Ogle, J. R. Creighton, S. Akhter, J. M. White, *ibid.* **169**, 246 (1986); N. R. Avery and N. Sheppard, *Proc. R. Soc. London Ser. A* **405**, 1 (1986).
6. T. A. Land, T. Michely, R. J. Behm, J. C. Hemminger, G. Comsa, *J. Chem. Phys.* **97**, 6774 (1992).
7. B. E. Bent, thesis, University of California, Berkeley (1986).
8. B. J. McIntyre, U. Schröder, M. Salmeron, G. A. Somorjai, in preparation.
9. T. A. Jung *et al.*, *Ultramicroscopy* **42–44**, 1446 (1992), and references therein.
10. M. Salmeron, R. Gale, G. A. Somorjai, *Phys. Rev. Lett.* **38**, 1027 (1977).
11. F. Zaera and G. A. Somorjai, *J. Am. Chem. Soc.* **106**, 2288 (1984).
12. J. H. Sinfelt, *Catal. Lett.* **9**, 159 (1991).
13. S. M. Davis and G. A. Somorjai, *J. Phys. Chem.* **87**, 1545 (1983).
14. B. E. Koel, B. E. Bent, G. A. Somorjai, *Surf. Sci.* **146**, 211 (1984).

15. The authors acknowledge U. Schröder for his technical assistance. This work was supported by the Director, Office of Energy Research, Office of Basic Energy Sciences, Materials Sciences Division, U.S. Department of Energy (DE-AC03-76SF00098).

20 April 1994; accepted 7 July 1994

A Redox Fuel Cell That Operates with Methane as Fuel at 120°C

Steven H. Bergens, Christopher B. Gorman, G. Tayhas R. Palmore, George M. Whitesides*

Platinum black efficiently catalyzes the oxidation of methane by iron(III) to generate carbon dioxide and eight equivalents of iron(II) in solutions of sulfuric acid in water. The rate of oxidation increases over 4 hours to reach ~4.83×10^{-2} moles of iron(II) per gram atom of surface platinum per second. A redox fuel cell was assembled that used this reaction in a liquid reformer to generate soluble reducing equivalents of iron(II) from methane, which was electrochemically oxidized to iron(III) in the cell. A vanadium(V)-(IV)–nitric acid–O_2 redox system catalyzed the electrochemical reduction of O_2. The open-circuit voltage of the cell was 0.48 volt, and the maximum power output of the cell was 8.1 milliwatts per cubic centimeter of graphite felt electrode.

We have operated a redox fuel cell with methane as fuel at 120°C in which graphite felt was used as the anode and cathode. Methane is presently the most abundant hydrocarbon fuel available (*1*). Because fuel cells are capable, in theory, of converting the free energy of oxidation of a fuel directly into electrical work without the thermodynamic limitations of a heat engine (*2*), the use of fuel cells to combust CH_4 is potentially an economical and efficient method of energy production. Unfortunately, the direct oxidation of alkanes in fuel cells is slow. The use of alkanes as fuels now requires that they first be steam-reformed to generate mixtures of H_2 and CO_2 so that H_2 can be used as a fuel in a conventional, H_2-O_2 fuel cell (*2*).

König, in a 1982 German patent, reported that Pt on graphite catalyzes the oxidation of CH_4 by $Fe_2(SO_4)_3$ in acidic water to generate mixtures of Fe(II), CO_2, and CH_3OH (*3*). It was difficult to prevent complete oxidation of CH_4 to CO_2, and a flow system was required to remove CH_3OH from Pt before further oxidation occurred. The König system is among the few robust systems that catalytically activates C–H bonds in the presence of functionalized molecules (H_2SO_4 in water) (*1*). Confirmation of the König report has not been reported, and rate, yield, and turnover data have not been obtained.

We have confirmed that the König system does catalytically activate C–H bonds under certain, reproducible conditions, and we have determined the rate and stoichiometry of the reaction under these conditions. Further, we circumvented the kinetic limitations of the direct electrochemical oxidation of CH_4 by using the König system as an intermediary redox catalyst that transferred electrons from CH_4 to the anode of a redox fuel cell (Fig. 1). We chose the König system because it operates under conditions similar to those in fuel cells (strong, aqueous acid) and because it effects the complete oxidation of CH_4. Although several reports have described redox catalysts in fuel cells that use H_2 (*4*), coal (*5*), and CO (*6*) as fuels, CH_4 has not been used previously to drive a redox fuel cell.

Methane was oxidized by Fe(III) with a catalytic amount of Pt black in a static reactor system [a T316 stainless steel bomb with a glass liner (*7*)] to generate CO_2 and eight equivalents (eq) of Fe(II) (Fig. 1) [1.02 mol % of Pt relative to starting

Department of Chemistry, Harvard University, Cambridge, MA 02138, USA.

*To whom correspondence should be addressed.

Fe(III); 0.6 M Fe(III) in 28 weight % H_2SO_4 in water; 120°C; CH_4 pressure (P_{CH_4}) = 54 atm; initial molar ratio of CH_4:Fe(III) = 42:1] (8). The rate of reaction increased over 4 hours to a maximum of ~4.83×10^{-2} mol of Fe(II) per gram-atom of $Pt_{surface}$ per second ($Pt_{surface}$ is an active site on the Pt black; the catalytically active surface of the Pt black was measured by H_2-O_2 titrimetry) (9).

A flow system was constructed that allowed the oxidation of CH_4 to occur in the bomb at high pressure and the redox fuel cell (Fig. 1) (*10*) to operate under ambient pressure. Oxidation of CH_4 in the bomb generated Fe(II) and CO_2, Fe(II) was reoxidized to Fe(III) at the anode of the fuel cell, and Fe(III) was returned to the bomb. A vanadium redox system [V(V)-V(IV)–HNO_3–O_2] (Fig. 1) (*11*) was used to catalyze the electrochemical reduction of O_2 in the cathode compartment of the cell. The electrical performance of the cell was similar to that of a related cell operating with MeOH as fuel (*12*).

Cell performance was maximized by running the reformer until most of the Fe(III) was reduced to Fe(II) before transferring electrolyte to the cell. A high ratio of Fe(II) to Fe(III) was then maintained in the electrolyte during operation of the cell by reforming CH_4 on a scale that produced Fe(II) at a rate higher than that of electrochemical oxidation to Fe(III) in the fuel cell and by continuously circulating electrolyte between the reformer and the anode compartment of the cell. At high currents, the cell voltage (E_{cell}) was constant while electrolyte was circulated between the reformer and the cell but dropped rapidly with concomitant change in color of the electrolyte from light blue (the color of $FeSO_4$ in aqueous sulfuric acid) to orange yellow [the color of $Fe_2(SO_4)_3$ in aqueous sulfuric acid] when circulation was stopped. Both E_{cell} and the light blue color of the electrolyte were restored when circulation of the electrolyte was restored. Mechanical difficulties (leaks and clogged filters, for example) usually prevented continuous operation of the cell for more than 3 hours.

The König system reproducibly activates C–H bonds efficiently and with good turnovers under the conditions shown in Fig. 1. The oxidation of CH_4 by Fe(III) is analogous to steam reforming except that the electroactive species generated from CH_4[Fe(II)] is highly soluble in the electrolyte. There are two intrinsic advantages of this liquid reformer over steam reformers: First, the operating temperature is lower (120°C versus 700° to 900°C) (*13*), and second, Fe(II) has high rates of electron transfer at carbon electrodes (the direct, electrochemical oxidation of H_2 gas usually is carried out with Pt as an electrocatalyst) (*2*). The primary limitation of the present liquid reformer is the loss of electrical energy during the oxidation of CH_4 by Fe(III) (~0.32 V, $E_{loss\ CH_4}$) (Fig. 1). We believe that this intrinsic thermodynamic limitation can be overcome to some extent by using redox couples with formal reduction potentials that are close to that of CH_4; the extent of the kinetic penalty for better matching of these potentials will have to be determined experimentally.

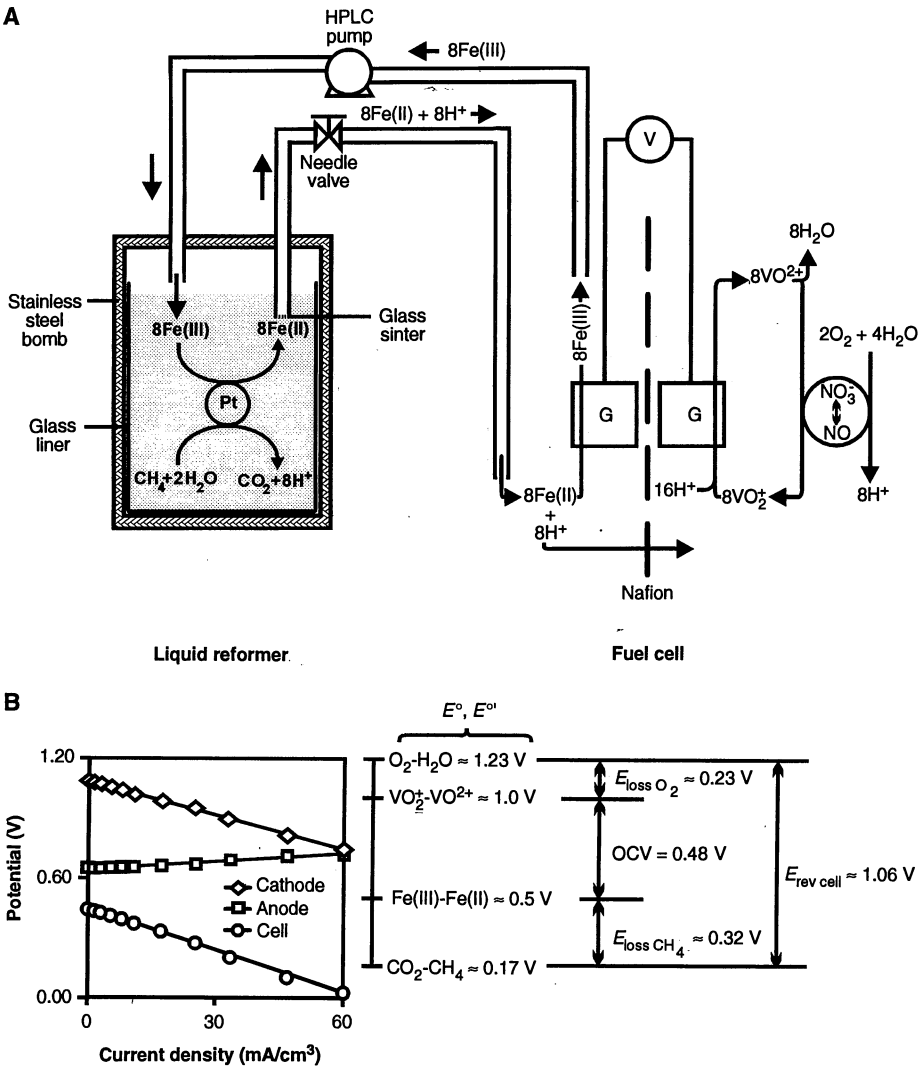

Fig. 1. (**A**) A schematic representation of the redox fuel cell operating with CH_4 and O_2. The liquid reformer section operated at 120°C under 54 atm of CH_4. The fuel cell operated at 80°C with the anode compartment under 1 atm of Ar and the cathode compartment under 1 atm of O_2. The needle valve was used to regulate the flow of anolyte from the bomb to the cell. The high-performance liquid chromatography (HPLC) pump was used to pump the spent anolyte from the cell back to the bomb. The anode and cathode consisted of graphite felt (G) that had been surface-oxidized by exposure to boiling, concentrated HNO_3 for 15 min. A platinum wire was used as current collector. (**B**) E_{cell} (○) (the potential difference across the cell), E_{anode} (□), and $E_{cathode}$ (◇) (E_{anode} and $E_{cathode}$ are versus standard hydrogen electrode and are not *IR*-corrected) are plotted against current density (per cubic centimeter of graphite felt) (*10*). The formal potentials of VO_2^+ ($E°_{VO_2^+\text{-}VO^{2+}}$) (*4*) and Fe(III) ($E°'_{Fe(III)\text{-}Fe(II)}$) (*11*), and the standard potentials of O_2 ($E°_{O_2\text{-}H_2O}$) (*15*) and CH_4 ($E°_{CO_2\text{-}CH_4}$) (*15*) are indicated. $E_{rev\ cell}$ is the potential difference across a reversible cell operating with CH_4 and O_2, $E_{loss\ CH_4}$ is the electrical energy lost during oxidation of CH_4 by Fe(III), $E_{loss\ O_2}$ is the electrical energy lost during reduction of O_2 by VO^{2+}, and OCV is the open-circuit voltage of the experimental cell.

REFERENCES AND NOTES

1. A. E. Shilov, *Activation of Saturated Hydrocarbons by Transition Metal Complexes* (Reidel, Dorecht, Netherlands, 1984); R. A. Periana *et al.*, *Science* **259**, 340 (1993); M. Lin and A. Sen, *J. Am. Chem. Soc.* **114**, 7307 (1992); D. A. Hickman and L. D. Schmidt, *Science* **259**, 343 (1993) and references therein.
2. L. Oniciu, *Fuel Cells* (Abacus, Kent, United Kingdom, 1976).
3. G. H. König, German patent De 3101024A1 (1982).
4. W. M. Carson and M. L. Feldman, *Proc. Annu. Power Sources Conf.* **13**, 111 (1959); J. T. Kummer and

D.-G. Oei, *J. Appl. Electrochem.* **12**, 87 (1982); *ibid.* **15**, 619 (1985).
5. A. M. Posner, *Fuel* **24**, 330 (1955).
6. J. M. Matsen, *Adv. Chem. Ser.* **64**, 277 (1967).
7. Parr Instruments, Moline, IL.
8. The Pt black (Aesar, fuel cell grade) was heated (185°C) under vacuum (0.03 torr) for 30 min before use. The $Fe_2(SO_4)_3$, H_2SO_4 (both Aesar, puratronic grade), and CH_4 (Matheson, ultrahigh purity) were used as received. Very high purity was required for the reagents to avoid catalyst poisoning. The water was deionized and doubly distilled. All solutions were deoxygenated, and the reactions were set up under 1 atm of Ar.
9. The dispersion of the Pt black (6.99%) was determined by titration with pulses of H_2 and O_2 (*14*). The rate of oxidation of CH_4 by Fe(III) was determined by bleeding aliquots of the reaction mixture through the needle valve and titrating them with Ce(IV). The rates obtained were approximate because the volume of solution decreased with each aliquot removed, which changed the mass transport properties of the reaction. We measured the amount of CO_2 by trapping it with a standard solution of $Ba(OH)_2$ (0.1 M) in water and then titrating the unreacted $Ba(OH)_2$ with a standard solution of HCl (0.1 M) in water. The amounts of Fe(II) and of CO_2 agreed within ±10%. No other products were detected in either the reaction mixture (analyzed by high-performance liquid chromatography with a Bio-Rad AMINEX column) or in the atmosphere of the bomb (analyzed by Fourier transform infrared spectroscopy and by gas chromatography mass spectroscopy).
10. The density and surface area of WDF graphite felt (Union Carbide) are 8.49×10^{-2} g/cm^3 and 0.5 m^2/g, respectively. We did not measure the surface area or the density of WDF graphite felt after it was treated with boiling, concentrated HNO_3. The geometric volumes of the electrodes (measured with a ruler) were used to calculate current densities. Because the electrodes are composed of thick porous felts, current densities are appropriately reported as volume densities (for example, milliamperes per cubic centimeter). The electrode chambers of the fuel cell were 3 cm in diameter and 5.5 cm deep. Each chamber contained a saturated calomel reference electrode. The chambers were separated by a Nafion 117 proton exchange membrane. The anode and cathode were rectangles of graphite felt that were 2 cm wide, 3 cm high, and 0.5 cm deep. The projected area of the anode and cathode on the Nafion membrane was 6 cm^2. The current collectors were Pt wires (0.5 mm in diameter and ~4 cm long) that were threaded through the graphite felt. Graphite rods can also be used as current collectors but with higher polarizations.
11. D.-G. Oei, *J. Appl. Electrochem.* **12**, 41 (1982).
12. S. H. Bergens and G. M. Whitesides, unpublished results.
13. P. Münster and H. Grabke, *J. Catal.* **72**, 279 (1981).
14. L. Carballo, C. Serrano, E. E. Wolf, J. J. Carberry, *ibid.* **52**, 507 (1978).
15. A. J. Bard, R. Parsons, J. Jordan, *Standard Potentials in Aqueous Solution* (Dekker, New York, 1985). We were unable to experimentally or theoretically determine the formal potentials of O_2-H_2O and of CO_2-CH_4. $E_{loss\ O2}$ and $E_{loss\ CH4}$ therefore only approximate the differences in formal potentials between O_2-H_2O and VO_2^+-VO^{2+} and between CO_2-CH_4 and Fe(III)-Fe(II).
16. This work was supported in part by the Advanced Research Projects Agency. S.H.B. thanks the National Engineering and Research Council of Canada for a postdoctoral fellowship. G.T.R.P. thanks the National Science Foundation for a postdoctoral fellowship. We thank both M. S. Wrighton and D. Maricle for useful discussions. R. Porcelli first pointed out the König patent to G.M.W.

25 March 1994; accepted 1 July 1994

A Spectroscopic Measurement of the Coronal Density of Procyon

J. H. M. M. Schmitt,* B. M. Haisch, J. J. Drake

One of the open key issues in the astrophysics of stellar coronae is the determination of their spatial structure and density. From almost all previous measurements, one can infer merely the presence of a corona, which for the most energetic stellar coronae may exceed the solar x-ray output by as much as five orders of magnitude, but no information can be obtained on the densities and hence volumes and sizes of the hot x-ray emitting material. A direct spectroscopic measurement of the coronal density was obtained for the star Procyon with the spectrometer on board the Extreme Ultraviolet Explorer satellite; the ratio of two Fe XIV lines at 211.32 and 264.79 angstroms was used to determine a density of ~4×10^9 to 7×10^9 electrons per cubic centimeter, which is a factor of 2 to 3 higher than typical solar active region densities. From this value, we estimate that ~6 percent of the stellar surface is covered with ~7×10^4 coronal loops.

The x-ray images of the sun obtained from Skylab (*1*), the Normal Incidence X-ray Telescope (NIXT) (*2*), and Yohkoh (*3*) have revealed an extremely complex structure in the solar corona. This structuring is the result of the confinement of the coronal plasma in magnetic loops, and in fact, most of the solar x-ray emission comes from a relatively small number of such loops spatially concentrated in active regions. Observations with the Einstein Observatory (*4*) and Roentgen Satellite (ROSAT) (*5*) telescopes have revealed x-ray emission from all classes of late-type stars except evolved K and M stars that are beyond the coronal dividing line (*6*). Does such emission originate in stellar analogs of solar active regions?

J. H. M. M. Schmitt, Max-Planck-Institut für Extraterrestrische Physik, 85740 Garching, Germany.
B. M. Haisch, Max-Planck-Institut für Extraterrestrische Physik, 85740 Garching, Germany, and Lockheed Solar and Astrophysics Laboratory, Division 91-30, Building 252, 3251 Hanover Street, Palo Alto, CA 94304, USA.
J. J. Drake, Center for Extreme Ultraviolet Astrophysics, University of California, Berkeley, CA 94720, USA.
*To whom correspondence should be addressed.

Stars cannot be spatially resolved, and thus, their coronal filling factors (that is, the fraction of their coronal volumes that emit x-rays) cannot be directly measured. Even in the rare cases of eclipsing binaries from which sizes of coronal structures can be inferred (*7*), it is impossible to distinguish between a diffusely filled structure and one in which the plasma is threaded through only a fraction of the volume. Heretofore, it has been impossible to determine whether, on a given star, coronal emission originates in rather compact high-density regions or in extended tenuous low-density regions because only the product of the square of the election density and the volume (that is, the volume emission measure, VEM = n^2V) could be determined from broadband flux or low-spectral resolution observations hitherto available. This dependence on n^2 arises from the dominant cooling process, that is, the excitation of ions by thermal electrons followed by radiative decay; because most of the gas is hydrogen, which is fully ionized at coronal temperatures, $n = 0.85n_e$, where n_e is the electron density. Consequently, spectroscopic measurements of n_e become of utmost importance because they can, in principle, be obtained for any coronal star, and from the VEM, which is directly derivable from the measured flux, the volume can be derived. Linear size scales of the x-ray emitting regions can then be determined on the basis of models of magnetic loops developed for the sun.

The star Procyon is a nearby astrometric binary consisting of a slightly evolved F5 IV-V star with a cool white dwarf companion. The x-ray emission from Procyon was first discovered with the Einstein Observatory's Imaging Proportional Counter (IPC) (*8*), which measured a luminosity of $L_x \approx 10^{28}$ ergs s^{-1}, about the same L_x as the sun at solar maximum. All of the observed x-ray emission was attributed to Procyon A (the F-type star), and the coronal temperature was found to be rather low (T_{cor} ~$10^{6.2}$ K) when compared with other stars with higher x-ray luminosity (*9*). On the other hand, because Procyon is slightly larger than the sun (radius $R_* \approx 1.9\ R_\odot$, where $R_\odot$ is the radius of the sun), the x-ray emission expressed as a surface flux is rather similar to that of the quiet sun, for which such a low T_{cor} would be appropriate.

Procyon has also been investigated with both the International Ultraviolet Explorer (IUE) and the European X-ray Observatory Satellite (EXOSAT). An extensive study of Procyon with IUE yielded the detection of a large number of chromospheric and transition-region lines (*10*); the ultraviolet line with the highest formation temperature is the N V line at 1240 Å with $T \sim 10^{5.2}$ K. The spectrum of Procyon obtained with the